This is a repository copy of *Objective phase-space identification of coherent turbulent structures in 1D time series*.

White Rose Research Online URL for this paper:
https://eprints.whiterose.ac.uk/191418/

Version: Published Version
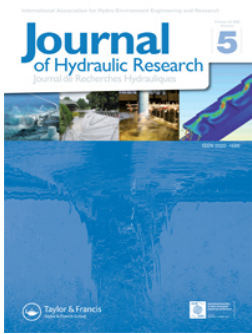
Article:

Objective phase-space identification of coherent turbulent structures in 1D time series

Jiayi Wu, Andrew Nichols, Anton Krynkin & Martin Croft

Published online: 08 Aug 2022.

Submit your article to this journal ↗

Article views: 220

View related articles ↗

View Crossmark data ↗

Research paper

Objective phase-space identification of coherent turbulent structures in 1D time series data

JIAYI WU [ORCID], PhD Student, *Department of Civil and Structural Engineering, University of Sheffield, Sheffield, UK*
Email: jiayi.wu@sheffield.ac.uk (author for correspondence)

ANDREW NICHOLS [ORCID] (IAHR Member), Senior Lecturer, *Department of Civil and Structural Engineering, University of Sheffield, Sheffield, UK*
Email: a.nichols@sheffield.ac.uk

ANTON KRYNKIN, Lecturer, *Department of Mechanical Engineering, University of Sheffield, Sheffield, UK*
Email: a.krynkin@sheffield.ac.uk

MARTIN CROFT, Managing Director, *Dynamic Flow Technologies Ltd, Unit 1, Loughborough Technology Centre, Loughborough, UK*
Email: martin@dynamicflowtech.com

ABSTRACT
Turbulent flow has been known to contain coherent flow structures. The size, shape, timescale and dynamics of these coherent structures are important in understanding turbulent flow processes such as pollutant mixing and particle transport. A range of methods exist for the detection of coherent structures in 2D or 3D data, but there are limited objective methods available for 1D data. Existing 1D techniques are subjective, require calibration with manual visualizations, or are based only on detecting velocity extremes and thus only detect structures according to a limited definition. A technique is presented here for objectively detecting structures using a phase-space method modified from a previously described despiking method. This method requires no calibration or subjective input, and identifies structures based on extremes in velocity, acceleration and jerk. This method gives turbulence statistics comparable with previous methods while recognizing a broader and more realistic definition of the physical properties of coherent structures by considering also the first and second derivative of velocity.

Keywords: ADV; coherent structures; flows in pipes; phase-space; U-level

1 Introduction

The study of turbulent flows is important in many fields of engineering and earth sciences. Turbulence in natural water flows controls many important physical processes, from the entrainment and transport of sediments to the mixing and advection of pollutants and the development of macrophyte populations. Originally, turbulence was considered as a statistically random process characterized by chaotic and unpredictable fluctuations, which were described via a turbulence spectrum (Zakharov et al., 1992). Leonardo Da Vinci was perhaps the first to propose that turbulent flows contain a series of discrete events that resemble eddies (Lozano-Durán & Jiménez, 2014) or whirls (Sarpkaya et al., 1994). More recently these have been

termed coherent flow structures (Ho & Huerre, 1984; Holmes et al., 1996; Hussain, 1986). Since coherent structures exist within the continuum of a flow field, there are conflicting definitions of what constitutes a structure and where the edge of a structure should be defined. Structures are generally considered to be vortex-like motions that can be oriented in any direction, and are characterized by extreme velocity, acceleration, and jerk (Eager et al., 2016; Schot, 1978).

The length, duration, occurrence frequency and advection velocity of coherent structures are key parameters to define when relating coherent structures to their effects on hydrodynamic processes such as mixing and sediment transport. Three dimensional velocity datasets (streamwise, lateral and vertical velocities) are usually measured in one, two or three

dimensional spatial locations. In this study, 1D, 2D, 3D refer to the number of dimensions in space and 1C, 2C, 3C refer to the number of velocity components measured. Thus, acoustic Doppler velocimetry (ADV) data are referred to as 1D 3C measurements. In the laboratory environment, 2D and 3D methods for measuring fluctuations in flow velocity or free surface elevation are becoming more commonplace, such as particle image velocimetry (PIV), laser-induced fluorescence (LIF), and particle tracking velocimetry (PTV). However, many studies still make use of 1D methods such as ADV (Caroppi et al., 2020), laser Doppler velocimetry (LDV) (Mohr et al., 2019), ultrasonic velocity profilometry (UVP) (Vargas et al., 2020) and conductive wave probes (Nichols, 2014). Further, 2D and 3D methods are usually considered too costly and complex for field applications such as *in situ* monitoring of river flows, with most studies opting for 1D methods such as ADV, acoustic Doppler current profilers (ADCP) (Guerra & Thomson, 2017) or electromagnetic current meters (ECM) (Creëlle et al., 2018). To extract the key parameters of coherent structures from 1D velocity data, a robust and objective detection technique is required. Existing techniques are subjective, require calibration with manual visualizations, or are based only on detecting velocity extremes and thus only detect structures according to a limited definition. This paper presents a new method, referred to here as the "phase-space method", to provide robust and objective coherent structure detection in 1D data. This can be used as an objective 1D detection method with similar statistics to the well-accepted U-level method, but with a more justifiable physical definition of a coherent structure.

This paper is organized as follows: Section 2 presents a summary of existing 1D techniques for coherent structure detection. Section 3 describes the experimental set-up and the measurement technique used in this study. Section 4 describes the phase-space algorithm developed for objective structure detection. Section 5 compares the result of the phase-space algorithm with the most established alternative. Finally, in Section 6, conclusions are presented.

2 Existing techniques

2.1 *Flow visualization*

Flow visualization is a straightforward method for investigating and understanding the physics of three-dimensional turbulence and dynamic fluid phenomena. Various visualization methods (e.g. dye injection or hydrogen bubbles) have been employed in numerous studies (Bogardt & Tiederman, 1986; Roy et al., 2004; Shvidchenko & Pender, 2001). Flow visualization has been proven to be useful for the identification of turbulent events and can provide a general description of the coherent flow structures (Head & Bandyopadhyay, 1981). However, since the method is based on a manual visual estimation, the output is highly subjective, and can only provide limited quantitative information on the characteristics of the turbulent

event (Boppe & Neu, 1995). The reliability of this technique reduces substantially when the Reynolds number is sufficiently large (Bogardt & Tiederman, 1986). In some studies, 1D detection techniques were calibrated against flow visualizations at relatively low Reynolds numbers, but the detection criteria cannot be reliably extrapolated to higher Reynolds numbers (Shah & Antonia, 1989). Besides, this technique can be laborious to employ in practice, as it requires a high degree of trial and error to effectively employ it (Smits, 2012) and it provides limited capability for quantitative measurements.

2.2 *Probe measurement with 1D techniques*

Considering the limitations of flow visualization, recent studies have been performed using probes to measure the velocity or pressure fields. With a reliable detection algorithm, probe measurements can be used to identify coherent structures in flows at much higher Reynolds number than is possible with flow visualization. Several measurement techniques have been used in laboratory and field studies, such as hot wire anemometry (HWA), laser Doppler anemometry (LDA), ECM and ADV. These probe measurements can provide a very good temporal resolution of 3D velocity fluctuations at a single position. Taylor's hypothesis can be invoked to turn time-resolved data to spatial data. This has been employed by many researchers in turbulent structure analysis, such as Boppe et al. (1999), Guerra and Thomson (2017), Ferraro et al. (2019), and Ng et al. (2021). The turbulence velocity fluctuation is assumed to be an ergodic process so that it is possible to use a sufficiently long time observation to reduce its statistical properties which are usually measured through a set of sufficiently large number of random realizations in multiple spatial locations.

To extract useful information from these velocity data, considerable effort has been given to the study of coherent structure detection techniques. 1D detection techniques (using time series of velocity or pressure recorded at a single spatial location) are the most straightforward, and are relatively simple to apply. They can also be applied not only to 1D data but also to 2D and 3D data by repeating the algorithm at different single points in the 2D plane or 3D volume. The most common 1D techniques for coherent structure detection are U-level (Bogardt & Tiederman, 1986), window average gradient (WAG) (Antonia & Bisset, 1990; Krogstad et al., 1998), VITA (Bogardt & Tiederman, 1986), Quadrant (Lu & Willmarth, 1973; Wallace, 2016) and TPAV (Wallace et al., 1977). These detection algorithms were found to be highly dependent on a user-defined threshold level and window size, which are often determined by a subjective comparison with flow visualization at low Reynolds number. The U-level algorithm (Lu & Willmarth, 1973) does not require a manually-defined threshold, and is therefore the only existing objective 1D detection method, but it only defines coherent structures according to a limited definition of extreme high or low velocity compared to the mean. The aim of this study is to propose a new objective method that more accurately

captures the physical nature of coherent structures, and compare this new method with U-level. The following sub-section describes the development of the U-level algorithm by several authors.

2.3   *U-level*

U-level is a relatively simple to implement technique for coherent structure detection, and the amount of data required for its use is minimal. It has been used in various previous studies such as Antonia and Bisset (1990), Baron and Quadrio (1997), Metzger et al. (2010), Nichols (2014), Vinuesa et al. (2015) and Tang et al. (2016). This technique looks at deficits from the mean streamwise velocity component and identifies extreme events as coherent structures. The U-level technique was first proposed by Lu and Willmarth (1973) for detection of burst-related events. An ejection event was assumed to occur whenever the velocity magnitude was below a certain threshold level:

$$u' < -k_U S_u \qquad (1)$$

where u' is the instantaneous streamwise velocity fluctuation, k_U is the threshold value and S_u is the root mean square of instantaneous streamwise velocity fluctuation over the measurement time period. Bogardt and Tiederman (1986) evaluated the effectiveness of this technique by comparing with dye flow visualization in a 60 mm by 575 mm rectangular channel at average velocity 0.129 m s^{-1}, depth 60 mm and Reynolds number 8200. When the threshold $k_U = 1$, the U-level technique gives 76% probability of detecting an ejection and 26% probability of a false detection. The threshold value k_U was then adjusted so that the number of events detected by U-level corresponded to the number of ejections identified by flow visualization, giving $k_U = 1.3$. This resulted in a U-level technique that appears to have a reasonably high probability of correctly detecting an ejection (63%) and a low probability of false detections (23%). Luchiktand et al. (1987) also analysed the effectiveness of the U-level technique with flow visualization. They confirmed that a higher threshold level leads to a lower probability of false detection, but also a lower probability of correct detection. Luchiktand et al. (1987) modified the U-level technique with an additional lower threshold to eliminate multiple detections of a single ejection or sweep and a sign to distinguish between ejections ($\alpha = -1$) and sweeps ($\alpha = 1$). The detector function was turned on and output D was set to 1 when:

$$u'\alpha < -k_U S_u \qquad (2)$$

and was turned off (output D was set to 0) when:

$$u'\alpha \geq -0.25 k_U S_u \qquad (3)$$

With the modification, Luchiktand et al. (1987) showed that the modified U-level technique had a substantial improvement in

the probability of detecting an ejection while the probability of false detection only increased slightly. Besides, it gave a reasonable estimate of the average duration of an ejection at a point in the flow. It is necessary to determine the appropriate threshold for the detection technique. Luchiktand et al. (1987) suggested that the threshold levels should be taken as the ratio between the absolute value of the long time average in the second quadrant $|\overline{u_2}|$ (where streamwise velocity fluctuation u' is negative and vertical velocity fluctuation v' is positive) and the standard deviation of velocity fluctuations S_u, thus:

$$k_U = \frac{|\overline{u_2}|}{S_u} \qquad (4)$$

Roy et al. (2004) and Nichols (2014) took the absolute value of velocity fluctuation instead of using the sign for detection of large-scale flow structures. The detection function was turned on when

$$|u'| > k_U S_u \qquad (5)$$

and off when

$$|u'| < 0.25 k_U S_u \qquad (6)$$

Taking the absolute value will give similar statistics but cannot distinguish between sweep and ejection events. The U-level method is not applied to each time step individually; the value (on/off) of each time step depends upon the value of the previous time step. Moving through from $t = 0$, the detector function is turned on when Eq. (9b) condition is met, and remains on for subsequent time steps until Eq. (9c) condition is met, at which point the detector function is turned off and remains so until Eq. (9b) condition is met again.

Despite the development of the U-level technique as an objective 1D method, it is still based upon the fundamental assumption that a coherent structure consists only of extreme velocity fluctuations. Coherent structures embody more than just extreme instantaneous velocities, and it can be argued they should be identified by also considering areas of high acceleration and jerk.

3   **Proposed phase-space algorithm**

Phase-space is a filtering technique commonly used in removing spikes from 1D data, proposed by Goring and Nikora (2002). This method plots the fluctuating component of velocity, its first order derivative with respect to time (acceleration) and its second order derivative (jerk) with respect to time in three-dimensional so-called phase-space axes. It assumes that all points lying outside an ellipsoid in the phase-space outliers (spikes), while points within the ellipsoid are valid data points. The size of the ellipsoid is determined by the universal threshold

λ:

$$\lambda = \sqrt{2 \ln N} \qquad (7)$$

where N is the number of data points. This method was shown to have better performance than various other methods and it has the advantage that it requires no external parameters which could otherwise introduce subjectivity.

As the phase-space method has no ambiguity in what threshold to choose, the present work has modified the method to enable detection of turbulent (extreme) events, events with extreme velocity, acceleration and/or jerk, rather than outliers. The steps of this new proposed technique, based on a measured steamwise velocity time series, u', are:

Step 1: Perform the standard phase-space despiking proposed by Goring and Nikora (2002) to remove erroneous data.

Step 2: Calculate the acceleration a_i and jerk j_i using the central difference method (Wu et al., 2005):

$$\Delta t = 1/f_s \qquad (8a)$$

$$a_i = \frac{u_{i+1} - u_{i-1}}{2\Delta t}, \quad i = 2, 3, \dots N - 1 \qquad (8b)$$

$$j_i = \frac{u_{i+1} - 2u_i + u_{i-1}}{\Delta t^2}, \quad i = 2, 3, \dots N - 1 \qquad (8c)$$

Step 3: Calculate the standard deviations of all three variables σ_u, σ_a and σ_j.

Step 4: Calculate the universal threshold according to Eq. (7).

Step 5: Transform the point cloud to be centred at the origin with no trend in any direction.

Step 6: Calculate the major, median and minor axes for the detection ellipsoid as:

$$e_u = k\lambda\sigma_u \qquad (9a)$$

$$e_a = k\lambda\sigma_a \qquad (9b)$$

$$e_j = k\lambda\sigma_j \qquad (9c)$$

where k is the phase-space scaling factor.

Step 7: Define the detection ellipsoid based on Eq. (10):

$$\frac{u'^2}{e_u{}^2} + \frac{a'^2}{e_a{}^2} + \frac{j'^2}{e_j{}^2} = 1 \qquad (10)$$

Step 8: Construct a binary series to signify the detection (or not) of turbulent events. Data points outside the defined ellipsoid (that satisfy Eq. 11) are recognized as 1 (detection of extreme event, termed as a "coherent structure data point" in this study), in the binary time series and data points inside the ellipsoid (that satisfy Eq. 12) are 0:

$$\frac{u'^2}{e_u{}^2} + \frac{a'^2}{e_a{}^2} + \frac{j'^2}{e_j{}^2} \geq 1 \qquad (11)$$

$$\frac{u'^2}{e_u{}^2} + \frac{a'^2}{e_a{}^2} + \frac{j'^2}{e_j{}^2} < 1 \qquad (12)$$

A sustained value of 1 in the binary series is defined as an individual turbulent event (coherent structure). Determine the number of individual turbulent events from the binary series. Roy et al. (2004) only considered events lasting more than 1 s from a modified U-level method while Nichols (2014) considered events of any time duration. Luchiktand et al. (1987) grouped two adjacent ejections, where the time between them was less than a threshold time value, into a single event. Shah and Antonia (1989) noted that the determination of the threshold time value is not totally free of ambiguity. To reduce the ambiguity of the proposed objective method, detected events of any time duration are all considered in this study. This also applies to modified U-level detected events to ensure consistency when comparing two methods.

Step 9: Use a value of scaling factor k ranging from 0 to 1 for step 6 to adjust the size of the ellipsoid.

Step 10: The value of k is chosen which gives the maximum number of turbulent events.

An example of these steps being applied to real laboratory data is given in Section 5.

4 Experimental measurement

The experiments were carried out in a 20 m long smooth circular pipe with 290 mm internal diameter and slope of 1/1000 (see Fig. 1 for the dimensions of experimental rig). Control of the discharge from the pump was achieved with an adjustable butterfly valve (a Fisher type 8580 [United States] butterfly valve with a type 2052 actuator) upstream of the inlet tank. The magnitude of the discharge was determined using an electromagnetic flow meter (Arkon MAG 910, Brno, Czech Republic). The depth of the flow was controlled with an adjustable gate at the downstream end of the pipe to ensure uniform flow conditions throughout the measurement section. The uniform flow depth d was measured with a point gauge at seven streamwise locations with average spacing 1.14 m. In this study, the flow depths ranged between 45.5 mm and 192.4 mm with bulk flow velocity U_b from 0.30 m s^{-1} to 0.60 m s^{-1}. The Reynolds number (computed by $\mathsf{R_e} = (\rho U_b R_h)/\mu_f$, where ρ is the water density, R_h is the hydraulic radius and μ_f is the dynamic viscosity of water) was between 0.84×10^4 and 5.05×10^4 as summarized in Table 1. The average depth is calculated as the mean of the water depth measured by point gauge at seven streamwise locations with average spacing 1.14 m before and
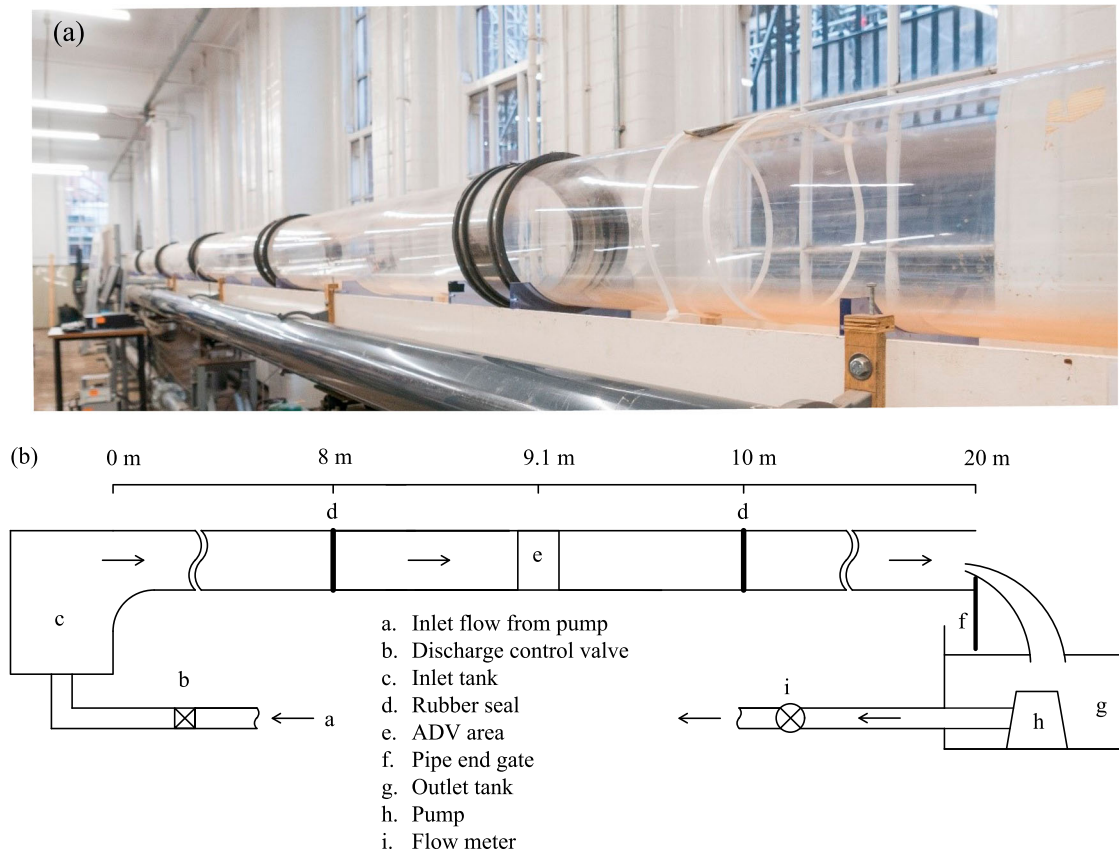
Figure 1   (a) A photograph of the pipe, and (b) sketch of the experimental set-up in this pipe showing the relative position of the measurement section with respect to upstream and downstream sections of the pipe

Table 1   Flow conditions

Flow condition	Flow rate, Q ($\mathrm{l\,s^{-1}}$)	Average depth, d (mm)	Bulk flow velocity, U_b ($\mathrm{m\,s^{-1}}$)	Reynolds number, $\mathrm{R_e} \times 10^4$ (–)
1	2	45.5	0.30	0.84
2	4	63.9	0.37	1.41
3	6	77.7	0.42	1.89
4	8	91.0	0.45	2.31
5	10	103.2	0.47	2.69
6	12	113.4	0.50	3.05
7	14	124.8	0.52	3.36
8	16	132.5	0.54	3.70
9	18	142.9	0.56	3.97
10	20	150.6	0.58	4.27
11	22	160.9	0.58	4.50
12	24	171.4	0.59	4.70
13	26	182.8	0.59	4.87
14	28	192.4	0.60	5.05

after the measurement area, and the bulk flow velocity is calculated by $U_b = Q/A$, where Q is the flow rate and A is the flow cross-sectional area. A side-looking ADV manufactured by Nortek (Norway) was used to measure the 3D instantaneous velocity time series at a given spatial point under uniform flow. It was mounted to a modified point gauge frame fixed at 9.1 m away from the inlet tank. The modified point gauge is able to adjust the depthwise position accurate to 0.1 mm. This type of instrument is frequently used in field and laboratory study (Cea et al., 2007; Clark & Kehler, 2011; Novo & Kyozuka, 2019) because of its reliability and robustness. In this study, ADV was sampled at 100 Hz and recorded by the software Vectrino Plus (https://www.nortekgroup.com/software) for a 300 s measurement duration. All measurements were made at least an hour after the flow was established to ensure the steady state of the flow. The background particles gave correlation over 80% on the ADV data, but 0.06% mass concentration of TiO2 was added to further improve reliability.

5   Results and discussion

5.1   *Phase-space detection*

ADV data are often contaminated by spikes (erroneous data points) as shown in Fig. 2a and it is essential to despike ADV data. All the ADV data in this study are despiked by the phase-space method proposed by Goring and Nikora (2002) first as mentioned in step 1 in Section 3. As is shown in Fig. 2, spikes are efficiently removed and replaced by cubic interpolation without altering the clean data. The velocity fluctuation was calculated from the velocity data measured by the ADV by subtracting the time-averaged value. It is known from Nichols (2014) that the frequency content of velocity time series in this type of flow is well below 10 Hz. For this data, the power spectrum calculated in MATLAB version R2019a (https://uk.mathworks.com/products/matlab.html) with function "fft" showed that the dominant components of the signal are well below 10 Hz. Therefore, the despiked velocity fluctuation data was low-pass filtered using a third order Butterworth filter with a cut-off frequency at 10 Hz to remove any risk of remaining high frequency noise. The filter would not affect the results apart from removing erroneous data points.

The data points for (u_i, a_i, j_i) were placed in the phase-space axes for values of i ($i = 3$ to $N - 2$). In order to fit the detection ellipsoid to a cloud of points with no bulk trend in any direction, the data points were first reduced to the $j = 0$ plane by subtracting the best fit plane from the jerk values and then reduced to the $j = 0$, $a = 0$ line by subtracting the best fit line from the acceleration. The equation of the best fit plane is obtained by the MATLAB "mldivide" function and the equation of the best fit line is obtained by the MATLAB "polyfit" function. Since the velocity values are already fluctuations about the mean, the centre of mass of the point cloud is now at (0, 0, 0) with no trend in any direction. After this detrend procedure, a detection ellipsoid centered at (0, 0, 0) without rotation can be defined. The sizes of principle axes of the detection ellipsoid were calculated from Eq. (9a) and the ellipsoid constructed using Eq. (10). Then the data points outside the ellipsoid were thus identified as coherent structure data points.

Next, the phase-space scaling parameter, k, was varied from 0 to 1 as described in Section 3, enlarging the ellipsoid from a single point to encompassing the full point cloud. As shown in Fig. 3a, the number of coherent structure data points detected as being turbulent begins with all data points when $k = 0$, and reduces to zero data points when $k = 1$. But the number of discrete events (continuous periods of positive detection) increases from 1 when $k = 0$ (one continuous event consisting of the entire time series), reaches a peak at some k value, and then decrease to zero when $k = 1$ (all data points within the ellipsoid, so no events detected). Similar plots are obtained for the other flow conditions and measurement positions. For the U-level method, the number of events detected increases with increasing threshold. U-level has a low probability of making a false detection as well as a low probability of a true detection when high

thresholds are used (Bogardt & Tiederman, 1986). Therefore, a compromise needed to be made in between the probability of making a false detection and the probability that an event will be detected, and an empirical threshold was settled upon subjectively. In case of the phase-space method, an appropriate threshold must also be determined. For this purpose, the value of the phase-space scale parameter k is chosen when it gives the maximum number of events (see Fig. 3b where the maximum number of events is indicated with the red marker). This represents the optimal sensitivity to detect extreme behaviour without merging discrete events. This provides an objective method for selecting the threshold, which yields turbulence statistics comparable with the accepted U-level method. This method was chosen because it provides a completely objective way of setting the threshold, which can be easily automated, and provides turbulence statistics comparable with U-level results.

The resulting phase-space detection using the optimal scaling parameter then enables construction of the optimal ellipsoid so that each point on the time series can be binarized as either (i) a coherent structure is present or (ii) a coherent structure is not present. The average value and standard deviation of the optimal scaling parameter for different flow conditions are calculated at all depthwise positions. The average scaling factor ranges from 0.294 to 0.308 for all flow conditions and the standard deviation is within 0.016. This small variation suggests a fixed value of the scaling factor ($k = 0.3$) may be appropriate for this particular flow system, but it is expected that different flow systems and application areas will exhibit different optimized scaling factors.

5.2   *Time series visualization*

Figure 4 shows the streamwise velocity, acceleration and jerk time series for a random 8 s segment of data. The red markers show where the U-level method detects an event and blue markers show where the phase-space method detected an event. Both methods can detect extreme velocity fluctuations (with U-level being more sensitive) while only phase-space can detect the extreme acceleration and jerk. At some time intervals, such as 5.83–5.93 s and 8.16–8.29 s, U-level does not detect an event because the velocity is not particularly extreme, but the phase-space method detects a high acceleration and/or jerk and identifies this as an event. Conversely, at some time intervals, such as 5–5.57 s and 10.27–10.37 s, U-level detects an event because the velocity magnitude is moderately high, but phase-space determines that the combined conditions of velocity, acceleration and jerk are not sufficiently unusual to be deemed a coherent structure event. In general, these two methods detect many of the same periods of events (for example 6–7 s, 7.5–9.8 s and 10.5–12.2 s) while the individual event durations differ. This is also observed by Krogstad and Kaspersen (1992) and Boppe and Neu (1995) when comparing different detection techniques. Similar plots are obtained for the other flow conditions, measurement positions and time sections. This occurs because
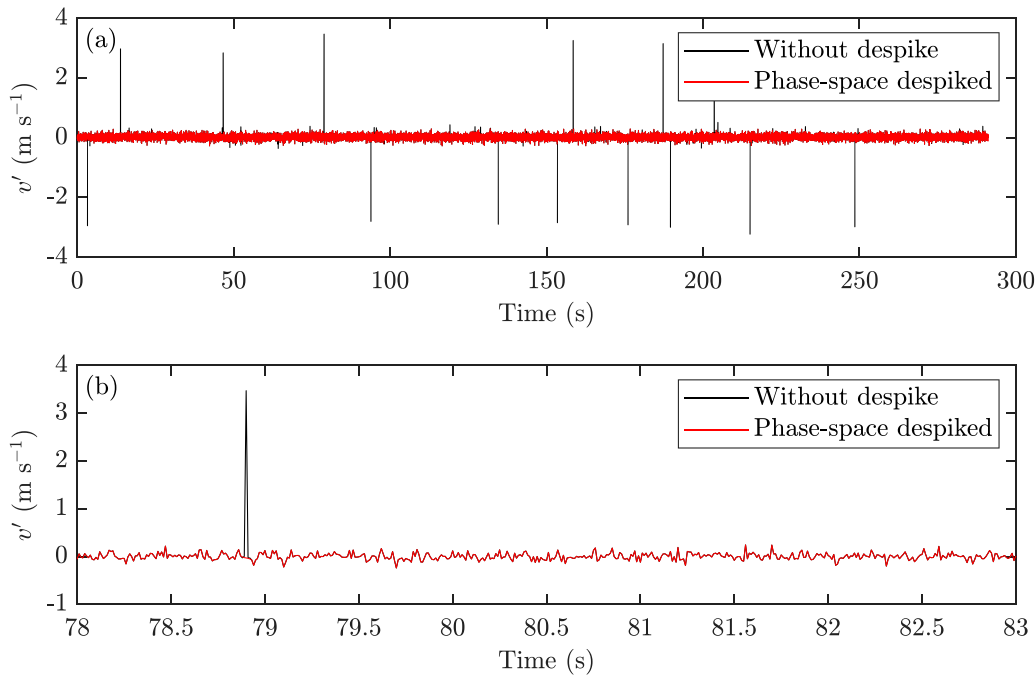
Figure 2   Time series for raw and despiked vertical velocity for flow condition 10 at depthwise position $y/d = 0.64$ (a) full 300 s (b) portion of 5 s
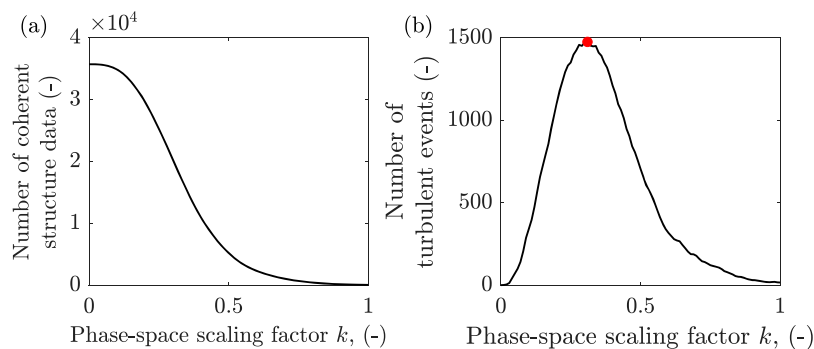

Figure 3   (a) Number of detected coherent structure data points versus the scaling factor; (b) number of detected discrete events versus the phase-space threshold, the red dot represents the maximum number of event. Time series analysis for flow condition 4 at depthwise position $y/d = 0.62$

U-level is more sensitive in order to produce event statistics similar to manual   visualization, while phase-space can be more refined, reflecting the physical reality that a coherent structure does not embody just extreme velocities.

5.3   *Phase-space axes analysis*

Figure 5 shows all the data points (u_i, a_i, j_i) on the phase-space axes. The data points not detected as part of coherent structure events are in black and the data points recognized as events are highlighted in colour (blue for U-level and red for phase-space). It is evident that the black points cluster in the centre of all data points for both methods. The points detected by the U-level algorithm are clearly delineated from the black points at two planes along the u-axis, while the points detected by the phase-space algorithm are outside the centre ellipsoid. Similar plots are obtained for the other flow conditions and measurement

positions. The abrupt threshold imposed by U-level appears rather aggressive and indiscriminate.

Figure 6 presents the phase-space projections of the data points detected by the U-level and phase-space algorithms (the point cloud viewed from three orthogonal directions). Data points highlighted in blue are points detected by U-level and points outside the ellipsoid (whose largest dimension is indicated by the ellipse) are points detected by phase-space. In the plot of number of coherent structure data points versus velocity u' distribution plot in Fig. 6a, the two algorithms aligns well in the extreme velocity region. However, no event data points are detected by the U-level algorithm when the velocity fluctuation is small in magnitude. In the plot of number of coherent structure data points versus a and j (Fig. 6d, e, f and h), the U-level algorithm shows a spike when the acceleration and jerk is small. Phase-space gives a more uniform detection towards the middle of the ellipsoid in all three
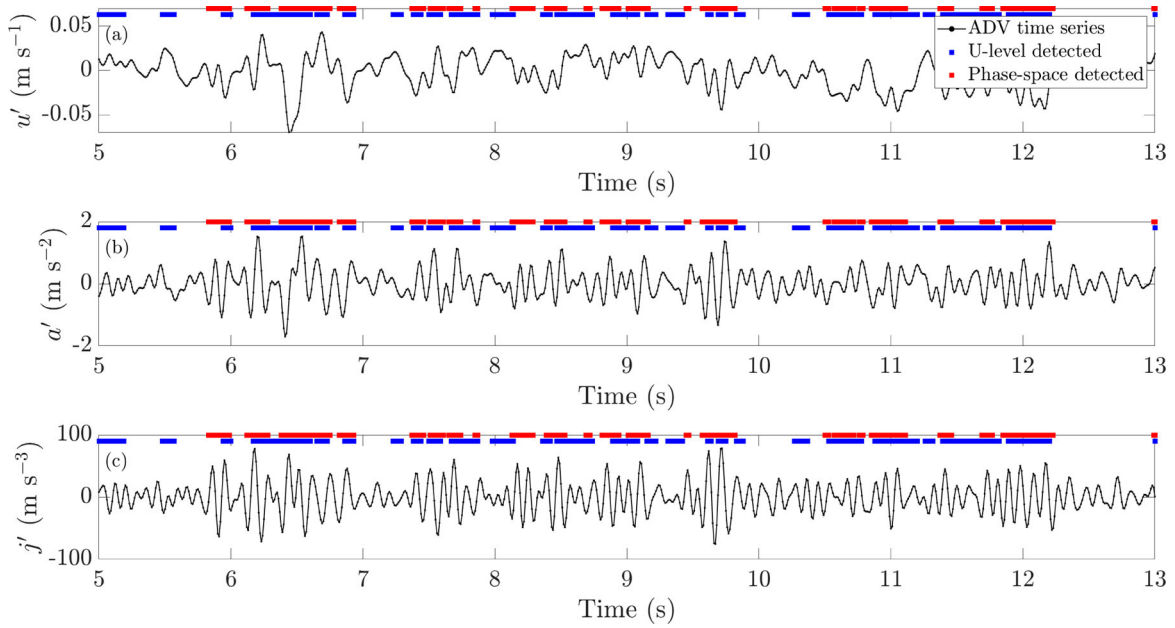
Figure 4   Time series of (a) velocity fluctuations; (b) acceleration fluctuations; (c) jerk fluctuations for flow condition 5 at depthwise position $y/d = 0.71$ (black lines represent velocity, acceleration and jerk time series respectively, blue markers are data points detected by U-level and red markers are data points detected by phase-space)
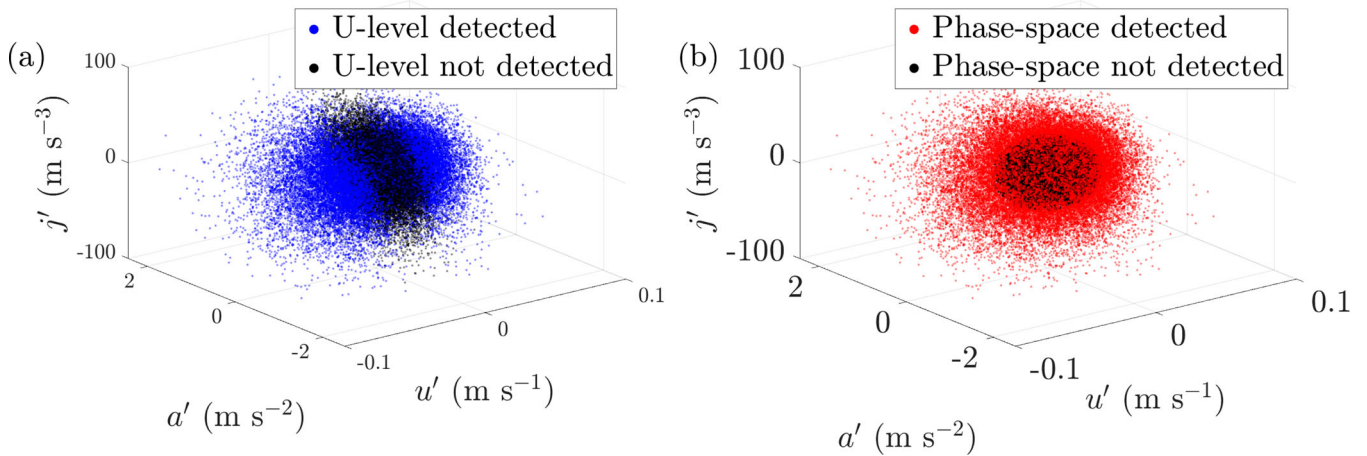

Figure 5   Data cluster in phase-space axes, coherent structure data points are in red/blue for flow condition 8 at depthwise position $y/d = 0.74$

directions, with detection appropriately reducing towards the edges. Similar plots are obtained for the other flow conditions and measurement positions.

5.4   *Evaluation in terms of turbulence parameters*

Figure 7 shows the histogram of the individual event duration ΔT and individual event period T_e from U-level and phase-space. Event duration is defined as the time between the leading and trailing edges of any continuous event, and event period is defined as the time interval of successive leading edges (Metzger et al., 2010; Tang et al., 2016). The two algorithms result in comparable histograms for both quantities. Exponential decay curves are fitted to the individual event duration plot as is shown in Fig. 7a since Bogardt and Tiederman (1986) showed that a histogram of time between ejections from flow visualization

analysis fits an exponential distribution. The probability density function of exponential fit is:

$$y_e = f\left(\Delta T | \mu\right) = \frac{1}{\mu} e^{\frac{-\Delta T}{\mu}} \tag{13}$$

where μ is the fitting parameter for exponential distribution. Gamma distribution curves are fitted to the individual event period plot as this more closely represents the histogram shape as is shown in Fig. 7b. The probability density function of gamma distribution is:

$$y_g = f\left(T_e | a, b\right) = \frac{1}{b^a \Gamma(a)} T_e^{a-1} e^{\frac{-T_e}{b}} \tag{14}$$

where a and b are fitting parameters for gamma distribution. The exponential and gamma fit is calculated using the MATLAB
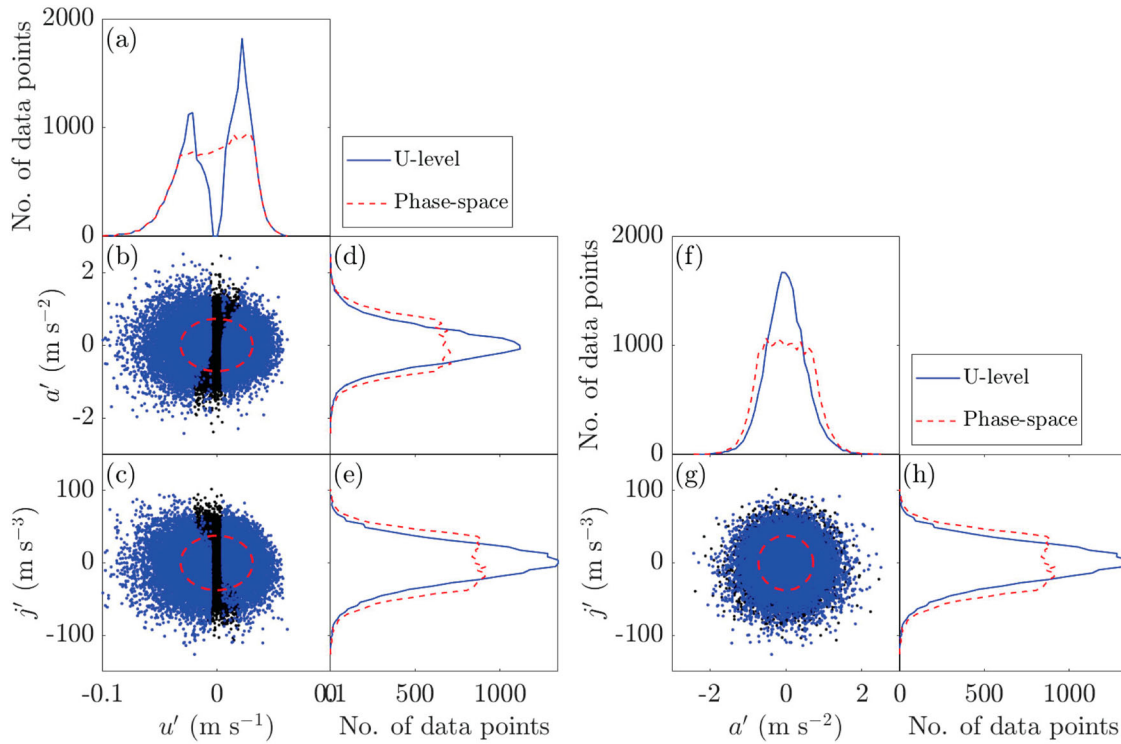
Figure 6   Coherent structure data point distribution for flow condition 5 at depthwise position $y/d = 0.66$

function "fitdist" with distribution name "Exponential" and "Normal" respectively. The average values of goodness of fit calculated by MATLAB function "goodnessOfFit" with cost function "NMSE" (normalized mean squared error) for all flow conditions and depthwise positions are approximately 0.93 for individual event duration and approximately 0.81 for individual event period, which means good fittings of histograms. The percentage difference of best fit probability density function parameters from U-level and phase-space is calculated by the value obtained from phase-space minus the value obtained from U-level and then divided by the value obtained from U-level. The difference in the best fit probability density function parameters μ, a and b from U-level and phase-space are generally less than 20% and phase-space shows lower values for all distribution parameters. The phase-space method histogram for individual event duration ΔT shows a skewness towards smaller values of ΔT, which is also observed by Bogardt and Tiederman (1986) and Metzger et al. (2010), who found that the histogram of individual event period T_e follows a Poisson-like distribution at any fixed normal location in the boundary layer, which demonstrates similarities with the histogram presented here. Similar plots are obtained for the other flow conditions and measurement positions.

Event duration and event period are significant in fluid dynamics analysis as event duration is associated with the structure length and the event period is associated with the frequency of turbulent occurrence. The agreement between the two methods shows that phase-space is able to accurately detect the
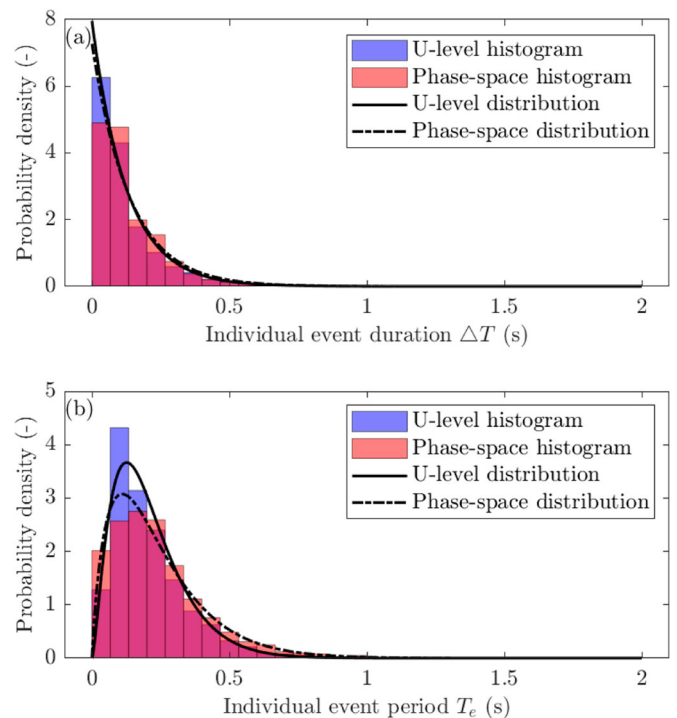

Figure 7   Normalized histograms of (a) individual event duration (b) individual event period for flow condition 10 at depthwise position $y/d = 0.64$

statistics of coherent events while being physically more justifiable in the detection criteria. The percentage difference in the number of events, event duration, mean individual event
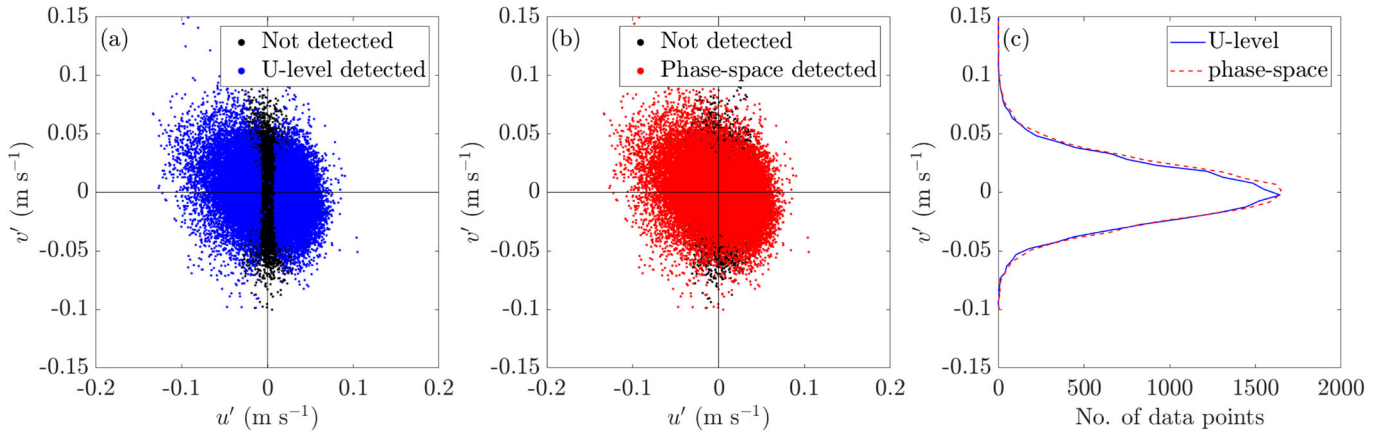
Figure 8   Detected coherent structure data points quadrant distribution for flow condition 6 at depthwise position $y/d = 0.339$ (a) U-level detection, (b) phase-space detection and (c) number of detected data points over vertical velocity direction

duration and mean individual event period are calculated by the value obtained from phase-space minus the value obtained from U-level and then divided by the value obtained from U-level. The number of events, e.g. the number of periods of successive values of 1 in the binary time series, from phase-space are usually more than from U-level by 39.66% on average. The percentage of total event duration is the ratio of the total number of 1 values in the binary time series and the length of the binary time series. On average, the percentage difference in total event duration is less than 1.03%. In terms of the time scale of events, both mean individual event duration and mean individual event period are lower from phase-space and the differences are 20.50% and 21.54% respectively. This corresponds to more structures being detected by the phase-space method, which are smaller in size than those detected by U-level.

5.5   *Quadrant axis analysis*

Figure 8 shows a quadrant plot (streamwise velocity fluctuation vs vertical velocity fluctuation). As shown in Fig. 8, it is evident that there are no coherent structure data points detected by U-level in the middle of the quadrant plot while phase-space detected points are more uniformly distributed, representing the physical reality that a coherent structure does not just depend on velocity in one direction. Similar plots are obtained for the other flow conditions and measurement positions. The distribution of coherent structure data points detected by the two methods over vertical velocity direction show comparable results. The percentage difference of the proportion of detected coherent structure data points in each quadrant is calculated by the value obtained from phase-space minus the value obtained from U-level and then divided by the value obtained from U-level. In general, phase-space shows 8.50% and 11.56% higher percentage of points in quadrants 2 and 3 while U-level shows 5.52% and 10.04% higher percentage of points in quadrants 1 and 4. That means more ejection (Q2) and inward interaction (Q3) events are detected by phase-space while more outward interaction (Q1) and sweep (Q4) events are detected by U-level.

Table 2   Percentage of a coherent structure data points being detected for all flow conditions

	Average (%)	Standard deviation (%)
U-level only (%)	15.92	0.65
Phase-space only (%)	16.49	0.50
Both methods (%)	40.85	0.91
Neither methods (%)	26.74	0.93
Agreement (%)	67.59	0.57
Disagreement (%)	32.41	0.57

5.6   *Binary series analysis*

Table 2 shows the percentage of coherent structure data points being detected by each method, by both methods, and by neither method. It also shows the agreement of the two algorithms (sum of points detected by both methods or neither) and the disagreement of the two algorithms (sum of points detected exclusively by each method only). The percentages are averaged over all the depthwise positions and the average and standard deviation for all flow conditions are summarized in Table 2. All standard deviation values are less than 0.93%, which means the performance of these two methods are consistent for all flow conditions. There are 15.92% and 16.49% data points that are only detected by U-level and phase-space respectively. The points detected by one algorithm but not the other are not surprising, since the proposed method uses an entirely different detection criterion to the established U-level method. There are 40.85% of coherent structure data points detected by both algorithms and 26.74% of data points are not detected as coherent structures by either algorithm. That together means these two algorithms show 67.59% agreement and 32.41% disagreement. Again, this is not surprising, since the phase-space method employs a more physically realistic definition of a coherent structure, whereas the U-level method only detects based upon extremes in velocity.
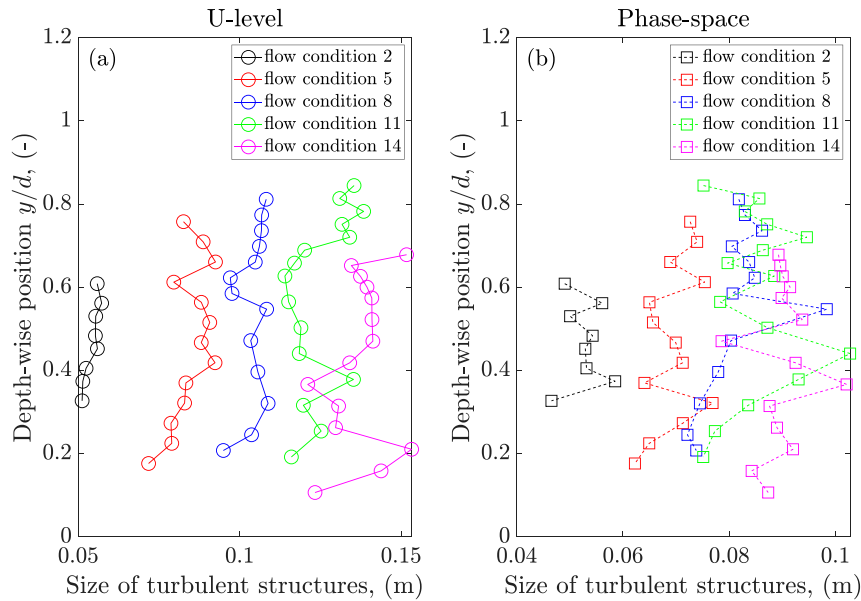
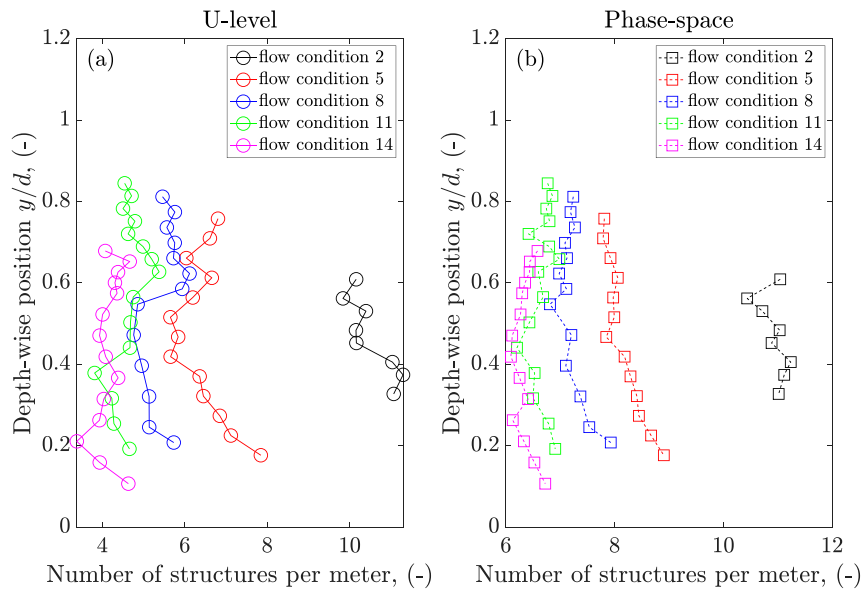Figure 9   Size of turbulent structures profile by (a) U-level, (b) phase-space

Figure 10   Number of structures per metre by (a) U-level, (b) phase-space

5.7   *Turbulent event profile analysis*

The proposed phase-space method is applied to the ADV data for all depthwise positions and flow conditions. The relation between properties of coherent structures measured via the proposed method and the bulk flow conditions and measurement depthwise positions are presented in this section. Two turbulent event profiles are analysed: size of turbulent structure vs depthwise position (Fig. 9) and number of turbulent structures per metre (Fig. 10). The size of turbulent structure is the product of mean event duration and mean depthwise streamwise velocity. The number of turbulent structures per metre is calculated from the reciprocal of the product of the mean event period and mean depthwise streamwise velocity. As shown in Fig. 9, both methods show larger turbulent structures with the increase of

flow, which agrees with observations of Nichols (2014). This also accords with observations from Roy et al. (2004), which showed that the size of large-scale turbulent flow structure scale with depth of flow. Figure 10 shows that with the increasing of flow, fewer turbulent structures are apparent per metre, with a slight increase in number of turbulent structures per metre near the bed for high flows. This is in agreement with the findings of Ng et al. (2021), which observe more large scale motions and very large scale motions at the bottom of the pipe. Profiles by the two detection methods show similar trends while phase-space shows generally smaller size of turbulent structures and a larger number of structures per metre. This can be explained by the mean event duration and event period by phase-space being lower than U-level, as discussed in Section 5.4.
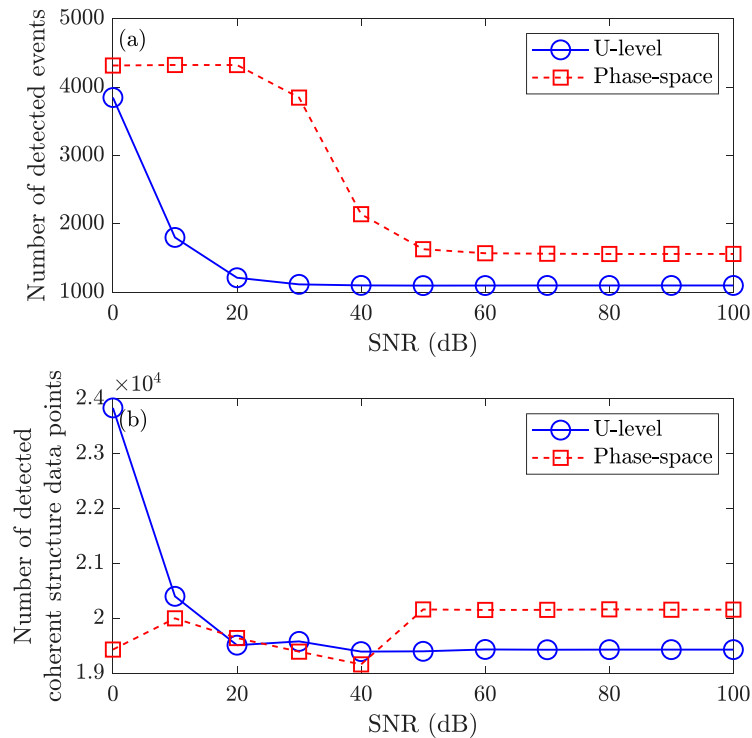
Figure 11   The performance of U-level and phase-space with different SNR (a) Number of detected events (b) Number of detected coherent structure data points

5.8   *Limitations*

The proposed phase-space method can be applied to any 1D velocity fluctuation data. The main weakness of the proposed phase-space method is that it is relatively more sensitive to noise. Different levels of artificial noise were added to ADV velocity data measured at flow condition 4 at depthwise position $y/d = 0.51$, with signal to noise ratio (SNR) ranging from 0 to 100. Figure 11 shows the performance of U-level method and phase-space method with different SNR in terms of number of detected events and number of detected coherent structure data points. U-level method results start to converge at 20 dB SNR while phase-space converge at 50 dB SNR. The phase-space method requires calculation of acceleration and jerk as indicated in Eq. (8a), which are easily affected by noise in velocity. Hence, the calculation of ellipsoid axes (Eq. 9a) and detection ellipsoid function (Eq. 10) are also affected. Therefore, use of the phase-space detection method is recommend for data with SNR greater than 50 dB.

6   Conclusion

This study proposed the use of a phase-space algorithm for turbulent event detection. This algorithm was compared with the U-level algorithm and evaluated in terms of the time series, phase-space axes, individual event duration, individual event period, quadrant contribution, binary series statistical similarities and turbulent event profiles. Results obtained can be summarized as follows:

- Phase-space coherent structure detection is an objective way to detect structures with no ambiguity in choosing the threshold value.
- The phase-space detected binary series is statistically comparable with U-level detected result. These two methods usually detect events in the same groups, but do differ slightly. Over 67% of data points can be detected by both methods or not detected by both methods.
- Turbulent event parameters can be obtained through the phase-space detected binary series and are comparable with U-level results.
- The relation between turbulent event parameters (the size of turbulent structures as well as number of structures per metre) and flow conditions can be observed by the proposed method.
- The phase-space method accounts for the physical reality that a coherent structure consists of extremes in velocity, acceleration and jerk, and that these properties should be considered together when identifying extreme behaviour.

These results confirm that the phase-space algorithm can be applied to 1D velocity data for detection of turbulent events. The employment of this algorithm will not only consider extreme velocity fluctuations but also extreme acceleration and jerk.

reviewers were very helpful in improving and clarifying the paper.

Notation

y	=	depthwise position (mm)
k	=	phase-space scaling factor (–)
d	=	water depth (mm)
u_2	=	second quadrant velocity ($\mathrm{m\,s^{-1}}$)
A	=	flow cross-sectional area ($\mathrm{m^2}$)
y_g	=	probability density function of gamma fit (–)
y_e	=	probability density function of exponential fit (–)
b	=	fitting parameter (scale) for gamma distribution (–)
a	=	fitting parameter (shape) for gamma distribution (–)
μ	=	fitting parameter for exponential distribution (–)
T_e	=	individual event period (s)
ΔT	=	individual event duration (s)
Q	=	flow rate ($\mathrm{l\,s^{-1}}$)
μ_f	=	dynamic viscosity of fluid ($\mathrm{kg\,m^{-1}\,s^{-1}}$)
R_h	=	hydraulic radius (m)
ρ	=	density of fluid ($\mathrm{kg\,m^{-3}}$)
$\mathrm{R_e}$	=	Reynold number (–)
U_b	=	bulk flow velocity ($\mathrm{m\,s^{-1}}$)
e_j	=	minor axis of the ellipsoid (–)
e_a	=	median axis of the ellipsoid (–)
e_u	=	major axis of the ellipsoid (–)
λ	=	universal threshold (–)
N	=	number of data points (–)
f_s	=	sampling frequency (Hz)
Δt	=	time interval (s)
u_i	=	streamwise velocity at ith step ($\mathrm{m\,s^{-1}}$)
σ_u	=	standard deviation of streamwise velocity ($\mathrm{m\,s^{-1}}$)
σ_a	=	standard deviation of streamwise acceleration ($\mathrm{m\,s^{-2}}$)
σ_j	=	standard deviation of streamwise jerk ($\mathrm{m\,s^{-3}}$)
j_i	=	streamwise jerk at i-th step ($\mathrm{m\,s^{-3}}$)
a_i	=	streamwise acceleration at ith step ($\mathrm{m\,s^{-2}}$)
λ	=	universal threshold (–)
v'	=	instantaneous vertical velocity fluctuation ($\mathrm{m\,s^{-1}}$)
u'	=	instantaneous streamwise velocity fluctuation ($\mathrm{m\,s^{-1}}$)
S_u	=	root mean square of instantaneous streamwise velocity fluctuation ($\mathrm{m\,s^{-1}}$)
k_U	=	U-level threshold (–)
α	=	sign of U-level (–)
D	=	U-level detection result (–)

ORCID

Jiayi Wu http://orcid.org/0000-0002-6807-620X
Andrew Nichols http://orcid.org/0000-0003-2821-621X

References

Antonia, R. A., & Bisset, D. K. (1990). Spanwise structure in the near-wall region of a turbulent boundary layer. *Journal of Fluid Mechanics*, *210*, 437–458. https://doi.org/10.1017/S0022112090001355

Baron, A., & Quadrio, M. (1997). Turbulent boundary layer over riblets: Conditional analysis of ejection-like events. *International Journal of Heat and Fluid Flow*, *18*(2), 188–196. https://doi.org/10.1016/S0142-727X(96)00087-2

Bogardt, D. G., & Tiederman, W. G. (1986). Burst detection with single-point velocity measurements. *Journal of Fluid Mechanics*, *162*, 389–413. https://doi.org/10.1017/S00221120 86002094

Boppe, R. S., & Neu, W. L. (1995). Quasi-coherent structures in the marine atmospheric surface layer. *Journal of Geophysical Research: Oceans*, *100*(C10), 20635–20648. https://doi.org/10.1029/95JC02305

Boppe, R. S., Neu, W. L., & Shuai, H. (1999). Large-scale motions in the marine atmospheric surface layer. *Boundary-Layer Meteorology*, *92*, 165–183. https://doi.org/10.1023/A:1001837729368

Caroppi, G., Västilä, K., Gualtieri, P., Järvelä, J., Giugni, M., & Rowiński, P. M. (2020). Acoustic Doppler velocimetry (ADV) data on flow-vegetation interaction with natural-like and rigid model plants in hydraulic flumes. *Data in Brief*, *32*, Article 106080. https://doi.org/10.1016/j.dib.2020.106080

Cea, L., Puertas, A. J., & Pena, A. L. (2007). Velocity measurements on highly turbulent free surface flow using ADV. *Experiments in Fluids*, *42*, 333–348. https://doi.org/10.1007/s00348-006-0237-3

Clark, S. P., & Kehler, N. (2011). Turbulent flow characteristics in circular corrugated culverts at mild slopes. *Journal of Hydraulic Research*, *49*(5), 676–684. https://doi.org/10.1080/00221686.2011.596399

Creëlle, S., Roldan, R., Herremans, A., Meire, D., Buis, K., Meire, P., Van Oyen, T., De Mulder, T., & Troch, P. (2018). Validation of large-scale particle image velocimetry to acquire free-surface flow fields in vegetated rivers. *Journal of Applied Water Engineering and Research*, *6*(3), 171–182. https://doi.org/10.1080/23249676.2016.1251856

Eager, D., Pendrill, A. M., & Reistad, N. (2016). Beyond velocity and acceleration: Jerk, snap and higher derivatives. *European Journal of Physics*, *37*(6), 1–11. https://doi.org/10.1088/0143-0807/37/6/065008

Ferraro, D., Coscarella, F., & Gaudio, R. (2019). Scales of turbulence in open-channel flows with low relative submergence. *Physics of Fluids*, *31*, Article 125114. https://doi.org/10.1063/1.5127562

Goring, D. G., & Nikora, V. I. (2002). Despiking acoustic doppler velocimeter data. *Journal of Hydraulic Engineering*, *128*(1), 117–126. https://doi.org/10.1061/(ASCE)0733-9429(2002)128:1(117)

Guerra, M., & Thomson, J. (2017). Turbulence measurements from five-beam acoustic doppler current profilers. *Journal of Atmospheric and Oceanic Technology*, *34*(6), 1267–1284. https://doi.org/10.1175/JTECH-D-16-0148.1

Head, M. R., & Bandyopadhyay, P. (1981). New aspects of turbulent boundary-layer structure. *Journal of Fluid Mechanics*, *107*(11), 297–338. https://doi.org/10.1017/S0022112081001791

Ho, C. M., & Huerre, P. (1984). Perturbed free shear layers. *Annual Review of Fluid Mechanics*, *16*, 365–424. https://doi.org/10.1146/annurev.fl.16.010184.002053

Holmes, P., Lumley, J. L., & Berkooz, G. (1996). *Turbulence, coherent structures, dynamical systems and symmetry*. Cambridge University Press.

Hussain, A. (1986). Coherent structures and turbulence. *Journal of Fluid Mechanics*, *173*, 303–356. https://doi.org/10.1017/S0022112086001192

Krogstad, P.-Å., & Kaspersen, J. H. (1992). Methods to detect coherent structures − a comparison. In *Australasian fluid mechanics conference* (pp. 1269–1272). University of Tasmania.

Krogstad, P.-Å., Kaspersen, J. H., & Rimestad, S. (1998). Convection velocities in turbulent boundary layers. *Physics of Fluids*, *10*, 949. https://doi.org/10.1063/1.869617

Lozano-Durán, A., & Jiménez, J. (2014). Time-resolved evolution of coherent structures in turbulent channels: Characterization of eddies and cascades. *Journal of Fluid Mechanics*, *759*, 432–471. https://doi.org/10.1017/jfm.2014.575

Lu, S. S., & Willmarth, W. W. (1973). Measurements of the structure of the Reynolds stress in a turbulent boundary layer. *Journal of Fluid Mechanics*, *60*(3), 481–511. https://doi.org/10.1017/S0022112073000315

Luchiktand, T. S., Tiederman, W. G., Luchik, T. S., & Tiederman, W. G. (1987). Timescale and structure of ejections and bursts in turbulent channel flows. *Journal of Fluid Mechanics*, *174*, 529–552. https://doi.org/10.1017/S0022112087000235

Metzger, M., McKeon, B., & Arce-Larreta, E. (2010). Scaling the characteristic time of the bursting process in the turbulent boundary layer. *Physica D: Nonlinear Phenomena*, *239*(14), 1296–1304. https://doi.org/10.1016/j.physd.2009.09.004

Mohr, L., Krick, T., Zimmer, M., Roder, T., & Muller, C. (2019). Fluid dynamic modeling and flow visualization of an industrial wet chemical process bath. *IEEE Transactions on Semiconductor Manufacturing*, *32*(3), 334–340. https://doi.org/10.1109/TSM.2019.2917083

Ng, H. C., Collignon, E., Poole, R. J., & Dennis, D. J. (2021). Energetic motions in turbulent partially filled pipe flow. *Physics of Fluids*, *33*(2), 025101. https://doi.org/10.1063/5.0031639

Nichols, A. (2014). *Free surface dynamics in shallow turbulent flows* [PhD thesis, University of Bradford].

Novo, P. G., & Kyozuka, Y. (2019). Analysis of turbulence and extreme current velocity values in a tidal channel. *Journal of Marine Science and Technology*, *24*, 659–672. https://doi.org/10.1007/s00773-018-0601-z

Roy, A. G., Buffin-Belanger, T., Lamarre, H., & Kirkbride, A. (2004). Size, shape and dynamics of large-scale turbulent flow structures in a gravel-bed river. *Journal of Fluid Mechanics*, *500*, 1–27. https://doi.org/10.1017/S0022112003006396

Sarpkaya, T., Merrill, C., & Carroll, J. (1994). *Coherent structures in vortex/free-surface interaction*. 32nd Aerospace Sciences Meeting and Exhibit, Reno, NV, U.S.A.

Schot, S. H. (1978). Jerk: The time rate of change of acceleration. *American Journal of Physics*, *46*(11), 1090–1094. https://doi.org/10.1119/1.11504

Shah, D. A., & Antonia, R. A. (1989). Scaling of the "bursting" period in turbulent boundary layer and duct flows. *Physics of Fluids A: Fluid Dynamics*, *1*, 318. https://doi.org/10.1063/1.857450

Shvidchenko, A. B., & Pender, G. (2001). Macroturbulent structure of open-channel flow over gravel beds. *Water Resources Research*, *37*(3), 709–719. https://doi.org/10.1029/2000WR900280

Smits, A. J. (2012). *Flow visualization – techniques and examples*. Imperial College Press.

Tang, Z., Jiang, N., Zheng, X., & Wu, Y. (2016). Bursting process of large- and small-scale structures in turbulent boundary layer perturbed by a cylinder roughness element. *Experiments in Fluids*, *57*, 79. https://doi.org/10.1007/s00348-016-2174-0

Vargas, D., Jayaratne, R., Mendoza, E., & Silva, R. (2020). On the estimation of the surface elevation of regular and irregular waves using the velocity field of bubbles. *Journal of Marine Science and Engineering*, *8*(2), 88. https://doi.org/10.3390/jmse8020088

Vinuesa, R., Hites, M. H., Wark, C. E., & Nagib, H. M. (2015). Documentation of the role of large-scale structures in the bursting process in turbulent boundary layers. *Physics of Fluids*, *27*, Article 105107. https://doi.org/10.1063/1.4934625

Wallace, J. M. (2016). Quadrant analysis in turbulence research: History and evolution. *Annual Review of Fluid Mechanics*, *48*, 131–158. https://doi.org/10.1146/annurev-fluid-122414-034550

Wallace, J. M., Brodkey, R. S., & Eckelmann, H. (1977). Pattern-recognized structures in bounded turbulent shear flows. *Journal of Fluid Mechanics*, *83*(4), 673–693. https://doi.org/10.1017/S0022112077001402

Wu, B., Bao, H., Ou, J., & Tian, S. (2005). Stability and accuracy analysis of the central difference method for real-time substructure testing. *Earthquake Engineering and Structural Dynamics*, *34*(7), 705–718. https://doi.org/10.1002/eqe.451

Zakharov, V. E., Falkovitch, G. C., & L'vov, V. S. (1992). *Kolmogorov spectra of turbulence I wave turbulence*. Springer.